Response to Referee #1 (RC2)

General Comments:

Entrainment is critical for the evolution of boundary layer. This study developed an approach for estimating entrainment zone thickness. Then this approach was applied to two cases. The evolution of boundary layer and entrainment zone thickness was analyzed at four stages. The difference between the winter and summer cases were also discussed. The topic is interesting but major revision is needed before I can recommend acceptance of this paper.

Authors' response:

We greatly thank this Referee for the thorough reading of the manuscript and encouraging comments on the current work. According to the Referee's valuable suggestions, all necessary modifications are made point by point in the revised manuscript.

Major comments:

1. Line 216-217: "Then, the upper and lower heights with half value of the maximum variance are searched and defined as the top and bottom heights of EZ, respectively." Why do the upper and lower heights with half value of the maximum variance represent the top and bottom heights of EZ? Please compare the top and bottom of EZ from this method with those from other methods to justify this method.

3. In section 4, only the results from this study are presented. Please compare these results with previous studies.

Authors' response:

(a) Along the Referee's suggestion, a new sentence "**Note here the FWHM of the variance profile of ABR fluctuations is utilized because it physically represents that most aerosols have been strongly mixed in the vertical height interval defined according to the FWHM**" has been added subsequently to state why the upper and lower heights with half value of the maximum variance represent the top and bottom heights of EZ (Please see Line 238 in the revised manuscript).

(b) We thank the Referee for suggesting validation of the EZT from the FWHM method. We believe this FWHM method to be physically sound as it directly reflects the mixing history of the aerosols (tracer) in the EZ. However, direct validation of the EZT retrievals is difficult as reviewed in the Introduction "**So far, no universally accepted approach exists for the determination of EZT**" and the existing approaches have their own deficiencies. A comparison with EZT result determined by its theoretical definition that corresponds to the vertical region with mean negative buoyancy flux might be favoured in future.

In response to the Referee's suggestions, a special paragraph including comparison with previous studies is now added to discuss on this issue in an added subsection "**4.3 Discussion on the clear-day EZT statistics and the FWHM method**". It reads "**Note the proposed FWHM method utilizes the FWHM of the variance profile of the ABR fluctuations to quantify the EZT. We believe it to be physically sound as it directly reflects the mixing history of aerosols (tracer) in**

the EZ. When applying it to lidar data, it definitely determines the EZ (and consequently the EZT) when turbulence is dominating and the variance profile of ABR fluctuations has clear-cut edges. However, caution must be taken when turbulence is weak and the variance profile of ABR fluctuations suffers from interference of residual layer and/or advected aerosols. The retrieved EZT values for the four typical clear-day cases mostly fall into the 50-150 m range with a percentage of ⩾67%, while the overall EZT values range from 0 to 340 m. Pal et al. (2010) reported the lidar-derived EZT retrievals for a summer case using the cumulative frequency distribution method, which had *mean* values of 75 m and 62 m and magnitude ranges of 10-230 m and 0-200 m for the quasi-stationary and growth stages, respectively. While for the early autumn case in this work, the EZT results had *mean* values of 113 m and 123 m and magnitude ranges of 41-279 m and 39-289 m for the quasi-stationary and growth stages, respectively. These observational results differ obviously for the *mean* EZT values and magnitude ranges. But this comparison seems not rigorous as the EZT results were obtained at distinct observational locations. For a better validation of the reliability of the FWHM approach, comparisons with EZT values retrieved by co-located intensive radiosonde or by synergy of high-resolution temperature lidar (Behrendt et al., 2015) and Doppler lidar (Ansmann et al., 2010), in which situation the EZT might be determined by its theoretical definition that corresponds to the vertical region with mean negative buoyancy flux (Driedonks and Tenneke, 1984; Cohn and Angevine, 2000), shall be favoured in the future".

2. Only two cases are analyzed to represent the results in winter and summer, respectively. To obtain robust conclusions, more cases are needed, at least, one month for each season. In addition, why do the authors only focus on winter and summer? Please include spring and autumn. The case on May 19, 2020 is actually a case in spring, not summer.

Authors' response:

We thank the Referee for suggesting more cases to yield robust conclusions. Two more clear-day cases have now been added in the revised manuscript. Besides, the case on May 19, 2020 is renamed as a later spring case. It is a pity that we failed to find a suitable clear-day case in summer months (June, July and August) due to rainy, and/or patchy-cloudy weather conditions. Instead, an early autumn case (on September 7, 2020) is selected as representative of a summer case since the surface temperatures (21-34 ℃) on this day were comparable with those on summer days (20-37 ℃; please refer to Table S3 in the Supplement for detail).

In response to the Referee's constructive suggestion, a new discussion subsection (**4.3 Discussion on the clear-day EZT statistics and the FWHM method**) has been added in the revised manuscript. Now the corresponding sentences read "**In combination with the above-two presented typical cases, another two clear-day cases (on the days of September 7 and November 12, 2020, respectively) are also investigated to demonstrate the robustness of the FWHM method and the representativeness of the conclusions on the EZ. The corresponding contour plots**

of the ABR, plots of the ABL depth and EZT evolution, as well as tables of obtained EZT statistics, are provided in the Supplement. Since no suitable clear-day case is available for the summer days of 2020 due to rainy and/or patchy-cloudy weather conditions, the early autumn result on September 7, 2020 is selected here and regarded as representative of a summer case as the surface temperatures on this day (21-34 ℃) were comparable with those on summer days (20-37 ℃; see Table S3 in the Supplement). Table 3 compares the EZT statistics for all the four picked cases.

As shown in Table 3, all four cases exhibited apparent statistical differences. For the same time interval of 0900-1900 LT, the winter case (case 1; a *mean* of 94 m, a *stddev* of 38 m) and the late autumn case (case 4; a *mean* of 103 m, a *stddev* of 48 m) had overall statistical EZT data smaller than those of the late spring case (case 2; a *mean* of 127 m, a *stddev* of 49 m) and the early autumn case (case 3; a *mean* of 113 m, a *stddev* of 60 m). Note this statistical conclusion was also true for each of the four developing stages. Besides, the winter case (8.5%) and the late autumn case (11.5%) had larger percentages of EZT falling into the subranges of 0-50 m than those of the late spring case (2.0%) and the summer case (8.0%), but smaller percentages (7.5% and 18.0%, respectively) of EZT falling into the subranges of >150 m compared to those of the late spring case (31.0%) and the summer case (24.0%). The reason of larger EZT statistics (*mean* and *stddev*) and higher percentage (possibility) of larger EZT values (>150 m) for the late spring and early autumn cases is attributed to the stronger solar radiation reaching the earth surface in late spring/early autumn than in winter/late autumn (Guo et al., 2020). Stronger solar radiation generally results in more vigorous and frequent thermals overshooting to higher heights (updrafts) and then moving back (downdrafts). Consequently entrainments take place in larger vertical regions. Hence both the EZT statistics (*mean* and *stddev*) and possibility of larger EZT value seem to provide measures of entrainment intensity. There were also common characteristics for the four observational cases. For example, all four cases showed moderate variations of *mean* of EZT from stage to stage. The growth stage always had the largest *mean* and *stddev* of EZT; as neither the NBL nor the FA restricts the booming development of the CBL in the growth stage, the entrainments were allowed to occur in a wider vertical range. Besides, the quasi-stationary stage usually had the smallest *stddev* of EZT; this quantitatively reflected the fact that the CBL depth and the EZT changed little in this stage. For all four stages, most EZT values fell into the 50-150 m subrange; the corresponding overall percentages of EZT falling into the 50-150 m subrange between 0900 and 1900 LT were 84%, 67%, 68% and 70.5% for the winter, late spring, early autumn and late autumn cases, respectively.”

Minor Comments:

1. In the introduction, please clearly state what is the deficiency of previous studies on this topic and what is new in this study.

Authors' response:

We really appreciate the Referee for the constructive suggestions on the Introduction part. Along these valuable suggestions, the sentences "**However, the above two introduced methods yield EZT values with large differences (e.g., Pal et al., 2010); the choice of specific percentages of air having the FA characteristics for the definition of EZ bottom height is variable (between 5% and 15%) among different researchers (e.g., Deardorff et al., 1980; Wilde et al., 1985; Flamant et al., 1997; Cohn and Angevine, 2000; Pal et al., 2010). Moreover, considering that variations of ABL depths can result from not only entrainment but also non-turbulent processes (e.g., atmospheric gravity waves and mesoscale variations in ABL structure), the methods depending on variations of ABL depth might not really characterize the true EZ (Davis et al., 1997). So far, no universally accepted approach exists for the determination of EZT (Brooks and Fowler, 2007)**" are added to review on the limitations of the current EZT determination approaches. Besides, the last paragraph of the Introduction part now reads "**Currently, studies are generally concentrated on the CBL while relatively rare on the EZ. The basic physical processes governing entrainment and their relationship with other boundary layer properties are still not fully understood (Brooks and Fowler, 2007). Besides, the general grid increments of state-of-the-art weather forecast and climate models are too coarse to resolve small-scale boundary layer turbulence (Wulfmeyer et al., 2016). Therefore, continuous and high-resolution measurements at various observational locations to infer detailed knowledge on both CBL and associated EZ, especially small-scale boundary layer turbulence therein, are of significant importance to boundary layer related studies including land-atmosphere interaction, air quality forecast and almost all weather and climate models (Wulfmeyer et al., 2016). In this work we present the high-resolution measurement results of the CBL and associated EZ using a recently-developed titled polarization lidar (TPL) over Wuhan (30.5°N, 114.4°E). The TPL is housed in a specially-customized working container and capable of operating under various weather conditions (including heavy precipitation). The TPL has an inclined working angle of 30° off zenith and routinely monitors the atmosphere with a time resolution of 10 s and a height resolution of 6.5 m. The equivalent minimum height with full overlap for the TPL is ~173 m above ground level (AGL). Based on the TPL-measured backscatter, a new approach has been developed for determination of the EZT. The small-scale characteristics of the CBL and associated EZ have also been investigated which can contribute to the improvement of understanding the structures and variations of the ABL, as well as parameterization of the EZ. The instrument, methodology, observational results and summary and conclusions are stated successively in following sections**" to state the meaning, significance and novelty of this work. We feel that the introduction part has been greatly improved after modification.

2. Line 214: ABR should be defined when it shows up for the first time.

Authors' response:

Along the Referee's suggestion, the ABR has been defined at an earlier place "**In this work the variance profile of aerosol backscatter ratio (ABR) fluctuations is calculated and the height with maximum variance is assigned as ABL depth**" (Please see Line 192 in the revised manuscript).

3. Line 242-246: Please give a figure to compare the ABR results.

Authors' response:

Following the Referee's suggestion, we have provided a Figure S1 as an example in the Supplement to compare the ABR results obtained by the two lidars on January 31, 2020. From this comparison figure, it can be seen that the concurrent ABR results by these two lidars generally had nearly identical structures and comparable magnitudes in the ABL region. Stronger ABR determined by the TPL at the near range (<400 m), can be explained by different viewing geometry (30°-off for TPL and vertical for another PL) and the higher height (~300 m) of complete FOV for another PL.

Supplement of

Measurement report: Characteristics of clear-day convective boundary layer and associated entrainment zone as observed by a ground-based polarization lidar over Wuhan (30.5 °N, 114.4 °E)

Fuchao Liu et al.

Correspondence to: Fuchao Liu (lfc@whu.edu.cn), Fan Yi (yf@whu.edu.cn)

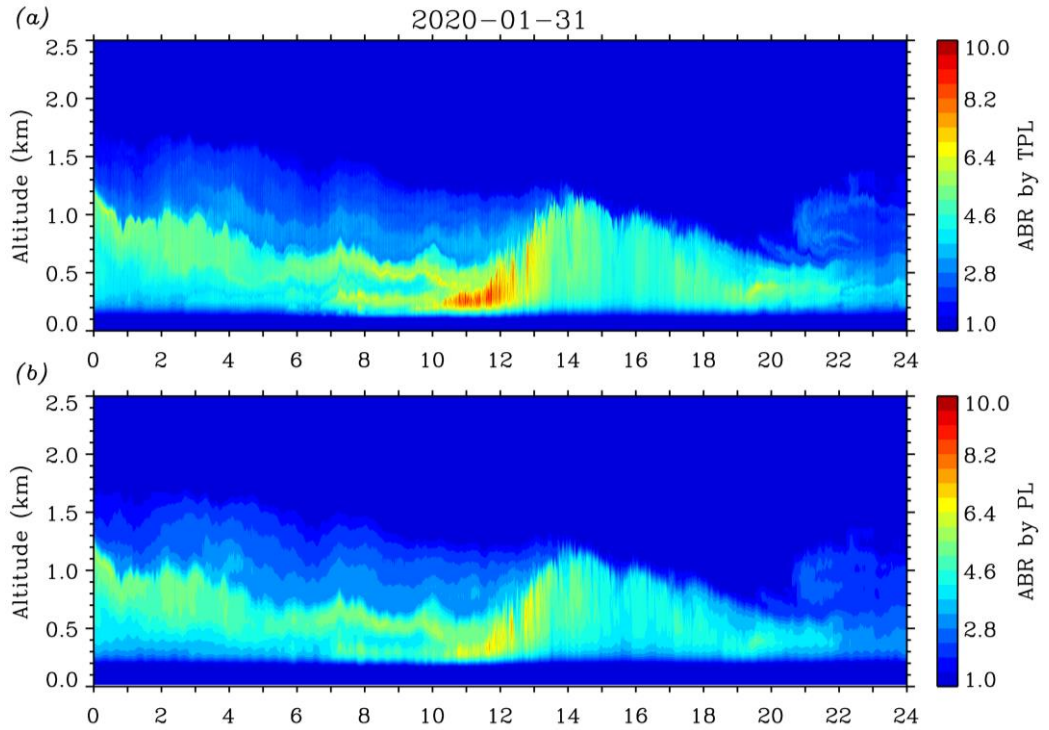

Figure S1: Contour plots of ABR results obtained by (a) the TPL in this work and (b) another co-located vertically-pointing 532-nm PL (Kong and Yi, 2015) on January 31, 2020. The TPL has 10-s temporal and 6.5-m spatial resolution, while the PL has 60-s temporal and 30-m spatial resolution. The two lidars have a horizontal range of ~15 m apart. Note the concurrent ABR results by these two lidars generally had nearly identical structures and comparable magnitudes in the ABL region.

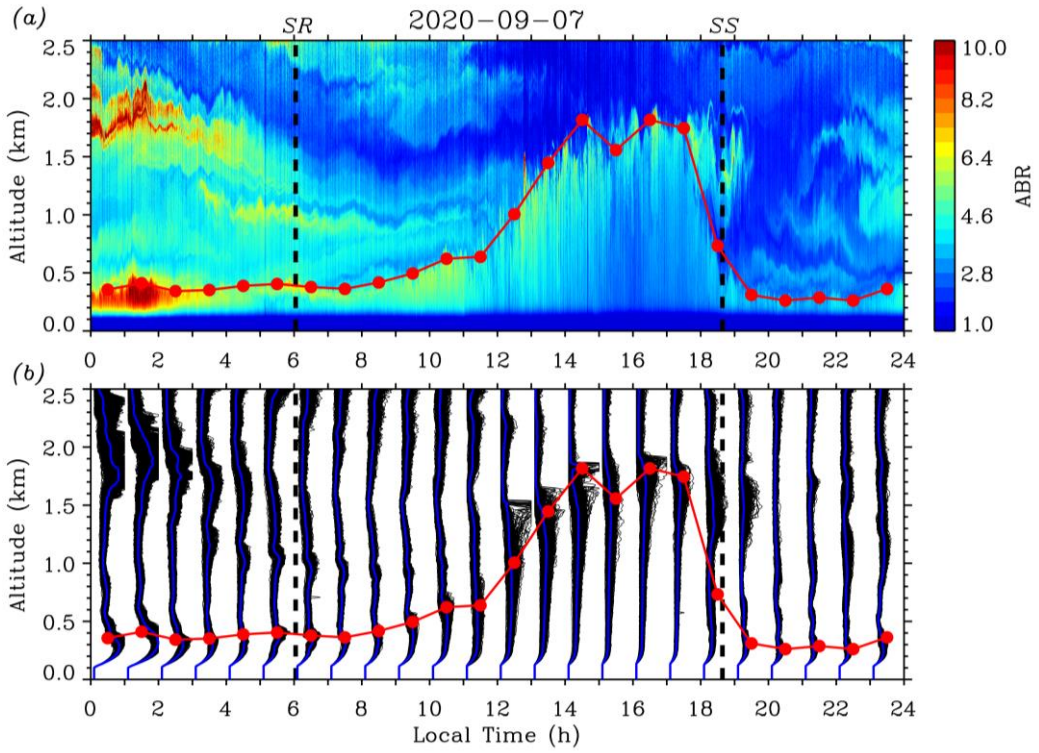

Figure S2: Same as Figure 4 but on the day of September 7, 2020.

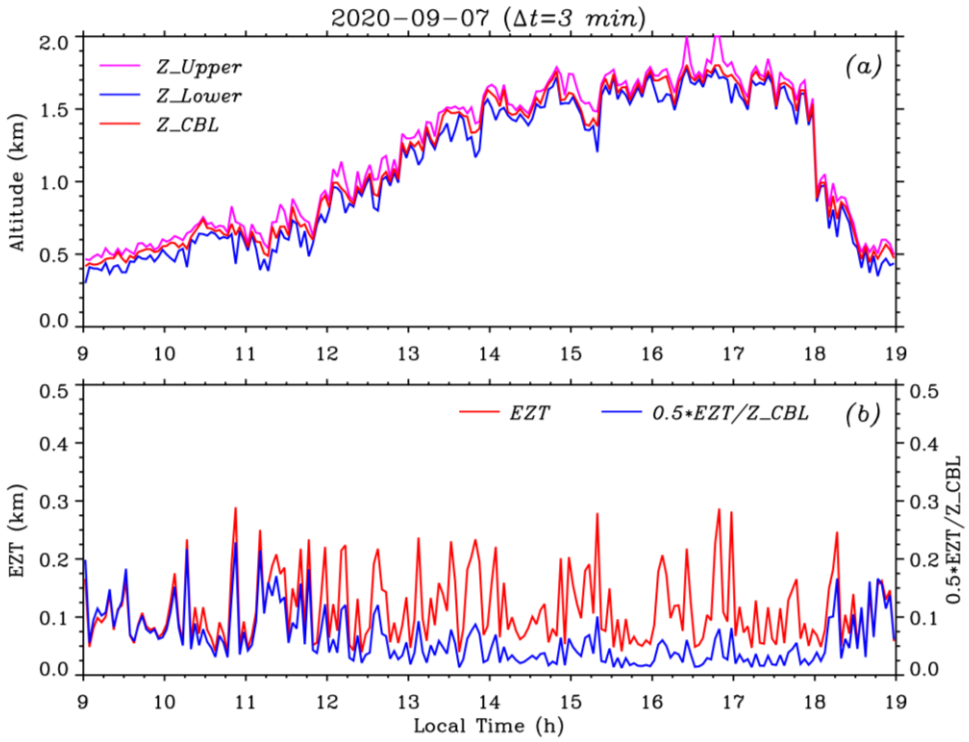

Figure S3: Same as Figure 6 but on the day of September 7, 2020.

Table S1: Statistics of EZT obtained on September 7, 2020

Stage of CBL		Formation	Growth	Quasi-stationary	Decay	Total
Time Interval (LT)		0900-1130	1130-1430	1430-1630	1630-1900	0900-1900
Statistical data of EZT(km)	*min*	0.039	0.039	0.041	0.034	0.034
	max	0.289	0.237	0.279	0.287	0.289
	mean	0.111	0.123	0.113	0.106	0.113
	stddev	0.058	0.062	0.057	0.060	0.060
Percentages in each EZT subrange (%)	0.00-0.05 km	10.0	6.7	5.0	10.0	8.0
	0.05-0.10 km	46.0	45.0	47.5	44.0	45.5
	0.10-0.15 km	20.0	18.3	22.5	30.0	22.5
	0.15-0.20 km	16.0	11.7	12.5	8.0	12.0
	0.20-0.30 km	8.0	18.3	12.5	8.0	12.0

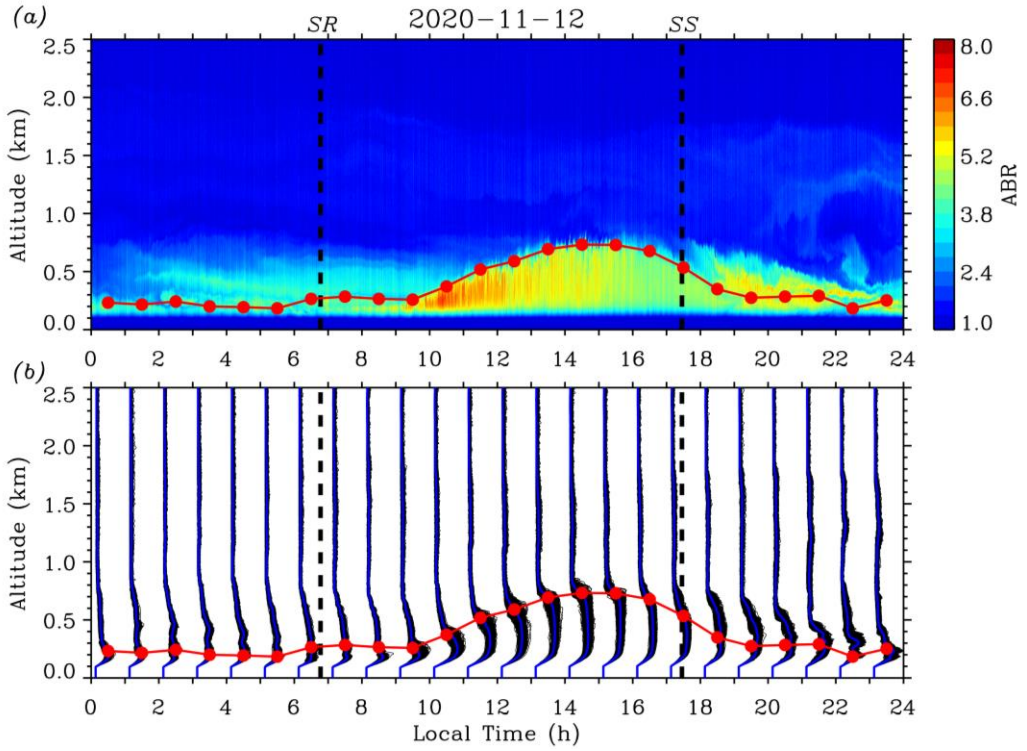

Figure S4: Same as Figure 4 but on the day of November 12, 2020.

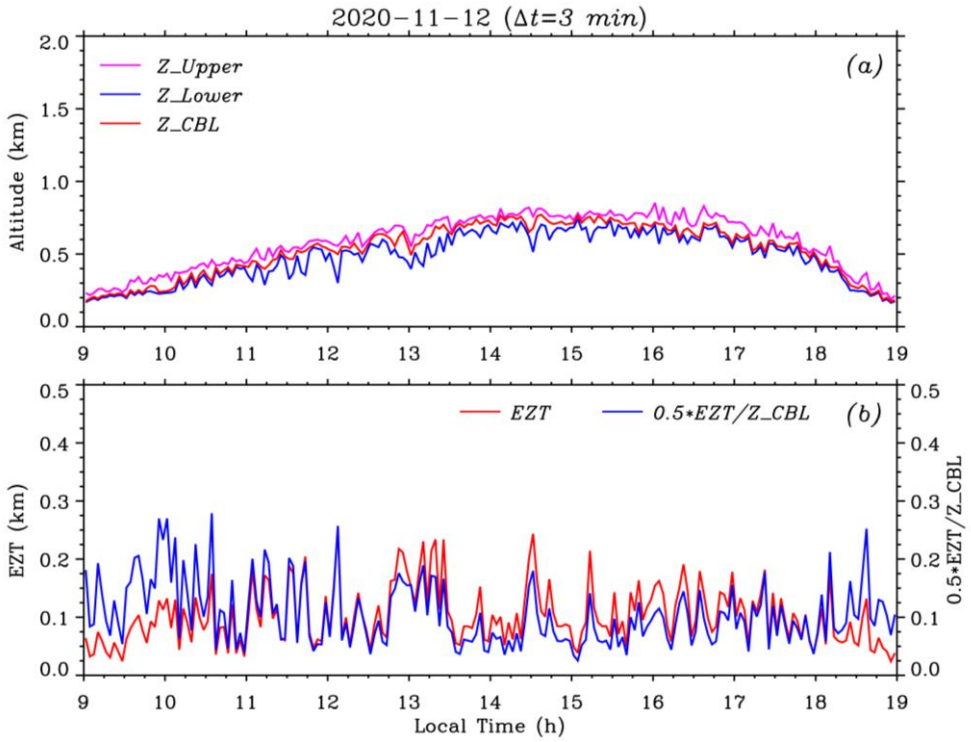

Figure S5: Same as Figure 6 but on the day of November 12, 2020.

Table S2: Statistics of EZT obtained on November 12, 2020

Stage of CBL		Formation	Growth	Quasi-stationary	Decay	Total
Time Interval (LT)		0900-1130	1130-1430	1430-1630	1630-1900	0900-1900
Statistical data of EZT(km)	*min*	0.024	0.043	0.039	0.024	0.024
	max	0.182	0.257	0.244	0.182	0.257
	mean	0.084	0.133	0.106	0.092	0.103
	stddev	0.041	0.062	0.040	0.042	0.050
Percentages in each EZT subrange (%)	0.00-0.05 km	22.0	5.0	5.0	14.0	11.5
	0.05-0.10 km	48.0	30.0	48.3	46.0	44.0
	0.10-0.15 km	22.0	22.5	28.3	32.0	26.5
	0.15-0.20 km	8.0	22.5	13.4	8.0	12.5
	0.20-0.26 km	0.0	20.0	5.0	0.0	5.5

Table S3: Surface temperature magnitude ranges for each month and the four typical days in 2020 over Wuhan (30.5 °N, 114.4 °E)

Month	Surface temperature magnitude range
January	-1-13 ℃ (0-13 ℃ for January 31, 2020; **Case 1**)
February	0-25 ℃
March	3-27 ℃
April	5-30 ℃
May	11-35 ℃ (18-29 ℃ for May 19, 2020; **Case 2**)
June	21-34 ℃
July	21-34 ℃
August	20-37 ℃
September	15-34 ℃ (21-34 ℃ for September 7, 2020; **Case 3**)
October	9-26 ℃
November	1-24 ℃ (7-22 ℃ for November 12, 2020; **Case 4**)
December	-6-16 ℃